EXW/P7-03

Recent Experiments of Lower Hybrid Wave-Plasma Coupling and Current Drive in EAST Tokamak

B J Ding 1), Y L Qin 1), W K Li 1), M H Li 1), E H Kong 1), A Ekedahl 2), Y Peysson 2), M Wang 1), H D Xu 1), H C Hu 1), G S Xu 1), J F Shan 1), F K Liu 1), Y P Zhao 1), B N Wan 1), J G Li 1), and EAST Group1)

1) Institute of Plasma Physics, Chinese Academy of Sciences, P R China, Hefei 230031

2) CEA/IRFM Cadarache 13108, Saint Paul Lez Durance, France

e-mail contact of main author: bjding@ipp.ac.cn

Abstract Using a 2MW 2.45GHz lower hybrid wave (LHW) system installed in EAST tokamak, LHW-plasma coupling and lower hybrid current drive (LHCD) experiments in both divertor configuration and limiter plasma have been performed systematically. Studies indicate that with the same plasma parameters, the best coupling is obtained in the limiter case, followed by the single null, and the last one is the double null configuration. RCs at different poloidal rows show that they have different coupling characteristics, possibly due to local magnetic connection length. Current drive efficiency has been investigated by a least squares fit, showing that there is no obvious difference in the drive efficiency between the double null and the single null cases, whereas the efficiency is a little small in the limiter configuration. The different current efficiency can be explained by the power spectrum up-shift factor. Current drive efficiency is affected by plasma density, mainly due to influence of density on impurity concentration. In addition, there is little dependence of drive efficiency on LHW power spectrum. The possible reason is that the temperature is low and LHW is absorbed after multi-pass propagation.

1. Introduction

Lower hybrid current drive (LHCD) has become an effective means to sustain tokamak plasma current and control plasma profile. A good LHW-plasma coupling is the first necessary condition for LHCD experiment and a high current drive efficiency is important for driving plasma current and controlling plasma current profile. Nuclear fusion experiments have made a rapid progress since 1980's in many tokamaks by using LHCD[1-8]. A 2MW 2.45GHz lower hybrid wave (LHW) system has been installed and run in Experimental Advanced Superconducting Tokamak (EAST), in which LHW-plasma coupling and LHCD experiments have been preliminary performed systemically recently.

Steady state operation and high performance are two main scientific goals of EAST. The comparisons of LHW-plasma coupling and current drive efficiency experiments in tokamak have not been reported yet. In order to pursue these tasks, it is necessary to investigate the

LHW-plasma coupling and LHCD experiment in different magnetic configurations in EAST so as to optimize the parameters of LHCD experiments.

2. Experiment setup

EAST is a first full superconducting tokamak with an advanced configuration in the world[9–13]. The EAST toroidal field system comprises 16 D-shaped toroidal field coils. The superconducting coils can create and maintain a toroidal magnetic field, B_t, of up to 3.5 T in steady state [13]. It can be run in the configuration of limiter, single null divertor (SN) and double null divertor (DN).

In EAST, a LHW is launched into the tokamak plasma by a multi-junction grill[14] type of antenna with 5 modules arranged by 5 rows in the poloidal direction. Each module consists of 4 main waveguides and each main waveguide consists of 8 active sub-waveguides between which there is a 90^0 phase difference generated by a built-in phase shifter. The power spectrum of the launched wave can be adjusted flexibly in the range of $1.85 \le N_{//}^{peak} \le 2.6$ when the phase difference between the adjacent waveguides of the coupler is feedback controlled at $-90^0 \le \Delta\Phi \le 180^0$, where $N_{//}^{peak}$ is the peak index of parallel refraction of the launched wave. In order to satisfy different coupling and current drive experiment, the LHW antenna can be moved in the range of ±15cm in the radial direction.

3. Experiments and results

3.1 LHW-plasma Coupling Characteristic

The LHW-plasma coupling experiments were performed in the DN configuration, the SN configuration and the limiter plasma (as shown in Fig. 1) with parameters of a plasma current (Ip)~ 250kA, a toroidal magnetic field (Bt)~2T, a central line averaged density (n_e) ~ $1.0\sim1.3\times10^{19}$ m^{-3}, and a peak value of parallel refractive index of $N_{//}^{peak}$ = 2.1. In the experiments, as also plotted in Fig. 1, the limiter and the LHW antenna are located at the major radius of $R_{Limiter}$=2370mm and $R_{Antenna}$=2376mm, respectively. The coupling is investigated by analyzing the input power (P_{in}), the reflected power (P_{re}), both of which are measured by directional couplers, and the averaged reflection coefficient ($RC = P_{re}/P_{in}$) over all the waveguides. The experiments were performed by changing the distance between the

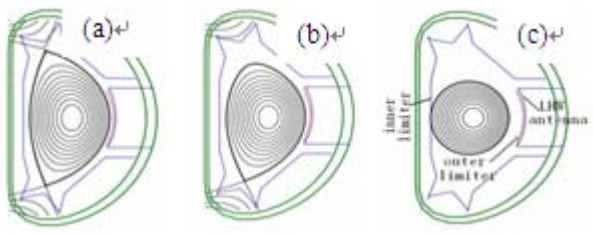

FIG. 1 Three configurations used in experiments
a. double null b. single null c. limiter

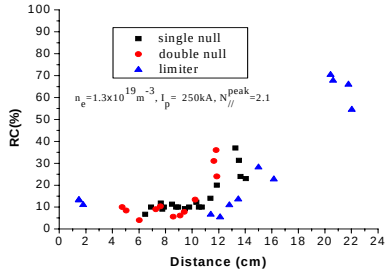

FIG. 2 Averaged RC vs distance between LHW antenna and LCFS

LHW grill and the last closed flux surface (LCFS) of plasma and investigating the coupling at different rows. The experimental results are shown in Fig. 2. It is seen that when the distance is less than 11cm, the averaged RCs over all rows with different configurations are almost the same (about 10%), suggesting that they have similar coupling characteristics. With the distance increase, there exists a turning point from which RC increases quickly, indicating the coupling deteriorates. Furthermore, the turning point value where RC increases is the smallest in the double null configuration, then followed by the single null configuration, and the largest one is the limiter case. The corresponding slope of RC increment with the distance exhibits the same variation tendency with RC, implying the dependence of coupling on distance is the strongest in the DN case, then the SN plasma, and the weakest is the limiter configuration. All the results suggest that the coupling in the limiter case is the best, the one in the DN case is the worst, and the one between them is the SN case.

The different coupling characteristics at 3 configurations can be interpreted by the different magnetic connection length L. Theory studies [14,15] indicate that the plasma density at the grill mouth ($n_{e,grill}$) and its gradient are two key factors determining the wave-plasma coupling. The grill-mouth density is determined by the distance d between the last closed flux surface (LCFS) and the grill mouth as follows [16] $n_{e,grill} = n_{e,LCFS} \cdot \exp(-\frac{d}{\lambda_{SOL}})$. Here, $n_{e,LCFS}$ and λ_{SOL} are the density at the LCFS and the decay length in the scrape-off layer, respectively. It is natural that the coupling deteriorates with the d increase since $n_{e,grill}$ decreases with increasing d. For an identical d, $n_{e,grill}$ is determined by λ_{SOL}, which is dependent of magnetic connection length L ($\lambda_{SOL} \propto L$). Let's consider the 3 configurations of limiter, single null and double null. For an identical plasma current and toroidal magnetic field, the length of L in the DN case is nearly twice of that in the SN case. Among the 3 cases, L in the limiter case is the largest. As a result, λ_{SOL} in this case is the largest, then the single null case, lastly the double null configuration. Therefore, the best coupling is obtained in the limiter case and the worst one is in the double null case. This can be seen from the edge density profile (see Fig.3) measured by Langmuir probes, showing that the density at the grill mouth (located at about Distance~5cm) in the limiter plasma is higher than that in the DN configuration. The experiment results are almost consistent with the simulations at different λ_{SOL} (see Fig. 4). Results show that RC first decreases with the increasing distance between plasma and LHW grill, and then increases with the distance, in agreement with the simulation through Brambilla theory.

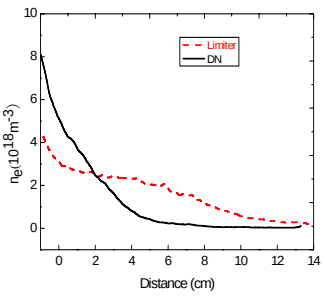

FIG. 3 Edge density profile

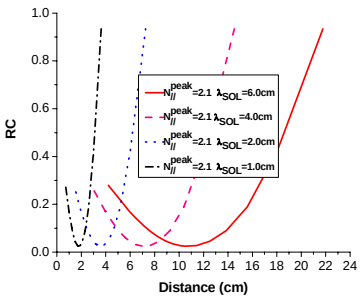

FIG. 4 Calculated RC vs distance

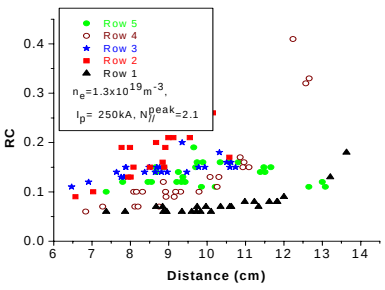

FIG.5 RC at different rows vs distance (SN)

The LHW-plasma coupling at different poloidal rows in the single null configuration is also investigated. As shown in Fig. 5, it is seen that for a same distance, the coupling in the first row is the best. The coupling in the 2nd row is the worst and the coupling is the most sensitive to the distance d in this row. There is no obvious effect of distance on coupling in the 5th row. The reason for the different coupling characteristics in different rows is not understood completely yet. Since magnetic connection is local and LHW-plasma coupling much depends on the connection length, it is inferred that the different sensitivity of coupling on distance may be ascribed to the different magnetic connection length.

3.2 Analysis of LHCD Efficiency

Based on the above coupling experiments, the current drive experiments have also been carried out for the three configurations (SN, DN and limiter) with B_t~2T. The dependence of plasma loop voltage and LHW power are investigated in the limiter plasma and plotted in Fig.6 (I_p~200kA, n_e~0.7×10^{19} m^{-3}, $N_{//}^{peak}$ = 2.1). It is shown the loop voltage (V_{loop}) drops quickly even with low level LHW power. With the increase of LHW power, especially when the loop voltage reaches zero, the effect of LHW power on loop voltage is not so sensitive. This is mainly because the interaction of electric field and fast electrons. Since LHW power is insufficient to sustain the total plasma current in the experiments, the plasma current is mainly sustained by LHW driven current, Ohmic current, and LHW-Ohmic synergy driven current. In this case, the current drive efficiency at zero loop voltage is estimated as follows.

Plasma current in the presence of both an inductive loop voltage V and an injected LHW power is expressed by[17, 18] $I_P = I_{ohm} + I_{RF} + I_{hot} + \ldots$ (1)

where I_{ohm} ($I_{ohm} = \frac{V}{R_{Sp}}$), I_{RF} ($I_{RF} = \frac{\eta_0 P_{LH}}{n_e R_0}$), I_{hot} ($I_{hot} = V/R_{hot}$) are the Ohmic current, the LHW driven current and the current due to interaction of LHW and Ohmic electric field. Here V is the plasma loop voltage, R_{Sp} is the Spitzer resistance [19], η_0 (defined as $\eta_0 = \frac{I_{RF} n_e R}{P_{LH}}$) is the current drive efficiency at zero loop voltage, P_{LH} is the absorbed LHW power, n_e is the plasma density, R is the major radius, and R_{hot} is the hot resistance [17], respectively. Note that I_{hot} is proportional to both the loop voltage and RF power [18].

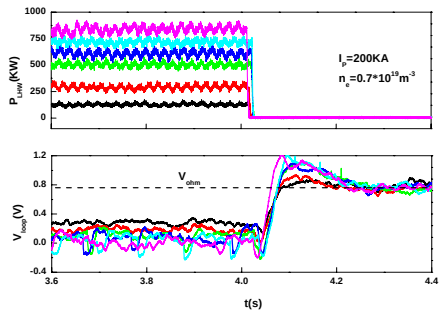

FIG.6 LHW power vs loop voltage

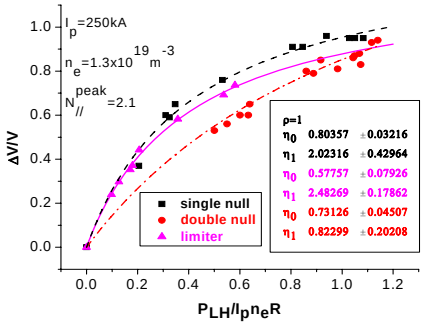

FIG.7 Relative change of loop voltage vs normalized LHW power

Without considering the temperature change due to the LHW application, equation (1) can be written as

$$-\frac{\Delta V}{V_{OH}} \equiv \frac{V_{OH}-V_{LH}}{V_{OH}} = \frac{(\eta_0+\eta_1)x}{1+\eta_1 x} \quad (2)$$

where V_{OH} is the loop voltage before the LHW application and V_{LH} is the loop voltage during the LHW application, $\eta_1 (= \frac{R_{Sp}}{xR_{hot}})$ is the synergetic current drive efficiency of LHW and Ohmic electric field, and $x (= \frac{P_{LH}}{n_e I_p R})$ is the normalized LHW power. With several power levels, Eqs. (2) can be used to determine η_0 and η_1 simultaneously, by means of a simple two parameter least squares fit, even if in the absence of data at $-\frac{\Delta V}{V_{OH}} = 1$.

For the 3 configurations, the experimental dependence of the relative drop of loop voltage ($\Delta V/V_{OH}$) on the normalized LHW power (P_{LH}/Ipn_eR) are plotted in Fig.7(I_p~250kA, n_e~1.0~1.3×10^{19} m^{-3}, $N_{//}^{peak}$ = 2.1), from which the non-inductive current drive efficiency has been obtained by the least squares fit. It is seen that there is no obvious discrepancy in the current drive efficiencies between SN (0.80×$10^{19}Am^2W^{-1}$) and DN (0.73×$10^{19}Am^2W^{-1}$) configurations, whereas the efficiency is a little small in the limiter case (0.58×$10^{19}Am^2W^{-1}$), suggesting the drive effect in the divertor configuration is better than that in the limiter case.
The different current efficiencies are in agreement with the simulated ray tracing and power deposition by LUKE/C3PO code. Figure 8 shows the poloidal ray trajectories and the parallel refractive index ($N_{//}$) evolutions during the ray propagation are shown in Fig.9, in which the wave accessibility [20] and the Landau damping condition ($6.5/T_e^{0.5}$) are also plotted. Where, s is the ray length and the black region means Landau damping through which the wave energy is transferred to electrons. It is seen that the Landau damping occurs after much longer ray path in the limiter case than that in the SN and DN plasmas, meaning the much slower absorption in the limiter plasma. This can be seen from the power evolution during the ray propagation shown in Fig. 10. As a result, no obvious difference in the power deposition between SN and DN configuration, and in the limiter case, the power deposition is near to core region with a little smaller power density, which can be seen in Fig.11, where r is the radial position and a is the minor radius.

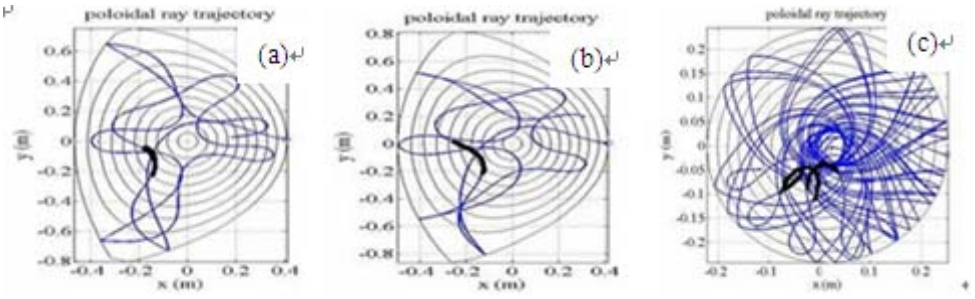

FIG. 8 Poloidal ray trajectory (a. double null b. single null c. limiter)

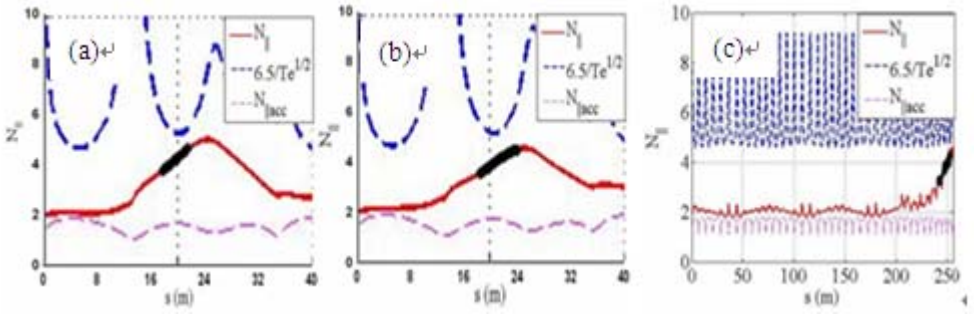

FIG.9 Evolution of parallel refractive index (a. double null b. single null c. limiter)

Usually, the theoretical current drive efficiency is calculated by [21] $\eta_0^{theor} = 1240\alpha/[\ln\Lambda(5+Z_{eff})(\beta^2 N_{//}^{\ 2})]$, where Z_{eff} is the effective nuclear charge number, α is the power absorption factor and β is the upshift factor of parallel refractive index at the power absorption point. According to the Karney-Fisch theory, there are two parameters proposed to describe the behavior of power flow in the presence of LHW and residual electric field. One is the ratio of poloidal magnetic field energy induced by LHW ($P_{el}=I_{RF}\times V$) to the absorbed LHW power by resonant electrons ($P_{abs}=\alpha P_{rf}$, P_{rf} is the injected LHW power), P_{el}/P_{abs}. The other is the ratio of LHW parallel phase velocity ($V_{ph}=c/(N_{//}\beta)$) to the electron runaway velocity(V_R), $u=V_{ph}/V_R$. The relation between P_{el}/P_{abs} and u is related by energy conversion function G(u) as follows[22]:

$$\frac{P_{el}}{P_{abs}} = \frac{\partial G/\partial u}{u} \qquad (3)$$

There are three regimes for u, which indicates the case of current decay, steady state, and ramp-up. According to Eq. (3), the numerical results with Z_{eff} =2 and Z_{eff} =5 (note that the typical values of Z_{eff} in this experiment locate between 2 and 5) are shown in Fig.12, in which the experiment data of P_{el}/P_{abs} and V_{ph}/V_R with the 3 configurations are fitted to theory curves. It is seen that the reasonable result is obtained at α=0.75 and the parallel refractive indexes at the point of power absorption are 4.7 (limiter), 4.1 (SN) and 3.7 (DN), nearly being in agreement with the simulations of the $N_{//}$ where Landau damping occurs. Since the data locate in the region of u < 0, it suggests that the LHW power is not enough for the full-drive current. This is the reason why the least square fit method is utilized to deduce the current drive efficiency at the zero loop voltage plasma.

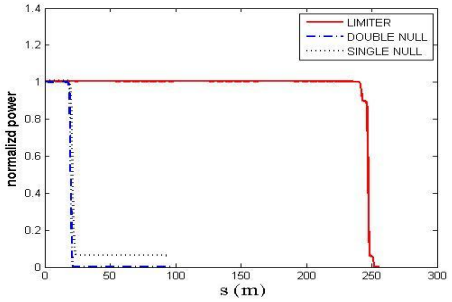

FIG. 10 Evolution of normalized LHW power during ray propagation

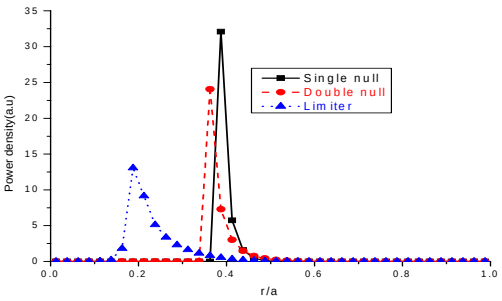

FIG. 11 Calculated power deposition (r is the radial position and a is the minor radius)

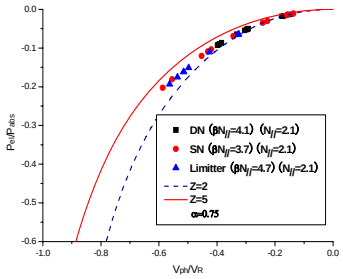

FIG. 12 P_{el}/P_{abs} vs V_{ph}/V_R

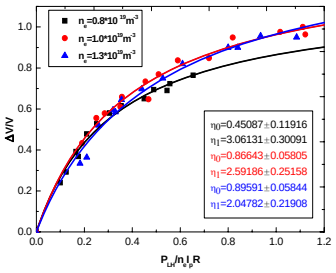

FIG. 13 CD efficiency vs n_e

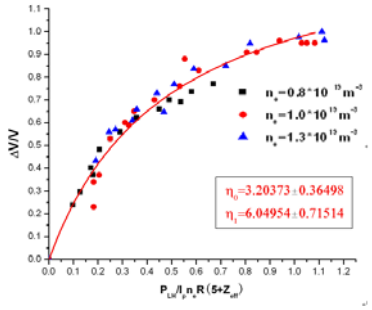

FIG. 14 Normalized CD efficiency

The current drive efficiency was also investigated with I_p~250kA and $N_{//}^{peak}$ = 2.1 at different density of 0.8×10^{19} m^{-3}, 1.0×10^{19} $m^{-3}$and 1.3×10^{19} m^{-3}. The obtained drive efficiencies are shown in Fig. 13, showing that the efficiency increases with the density increase. Simple estimation indicates the wave satisfies the accessibility condition. Invoked from $\eta_0^{theor} = 1240\alpha/[\ln\Lambda(5+Z_{eff})(\beta^2 N_{//}^{\ 2})]$, Z_{eff} is a possible candidate for the dependence of drive efficiency on density since Z_{eff} will decrease with the density increase. With the increase of Z_{eff}, impurity radiation increases, hence reducing driven current. In order to investigate it, the drive efficiency is normalized by $5+Z_{eff}$. Seen from Fig. 14, the data with the three densities are in line and it can be fitted by one curve. Therefore, the impurity concentration is the main reason for the discrepancy in the drive efficiency.

The current drive experiments have also been performed with different LHW power spectrum ($N_{//}^{peak}$ =1.85, 2.1, 2.35). As shown in Fig.15, it indicates that there is little dependence of drive efficiency on LHW power spectrum. The possible reason is that the temperature is low and LHW is absorbed after multi-pass propagation. As a result, the initial condition of spectrum does not play so important role. This could be improved in future high performance.

4. Discussion and Conclusion

The wave-plasma coupling and current drive experiments at different configurations are performed and analyzed systematically in EAST, suggesting that LHW can be effectively coupled into plasma and drive plasma current with present LHW system. Preliminary studies indicate that LHW-plasma coupling and current drive efficiency are both affected by plasma configurations. The best coupling is obtained in limiter configuration, then SN plasma, and the worst is DN plasma. Studies show that this is mainly due to the discrepancy in magnetic connection length. Results indicates that the coupling characteristic is different, suggesting the possible local characteristic of magnetic connection. The CD efficiency in limiter plasma is lower than those in divertor configurations, suggesting that CD efficiency is affected by plasma configuration. This is mainly because the ray race much depends on configuration, leading to different ray length before Landau damping and upshift factor of refractive index,

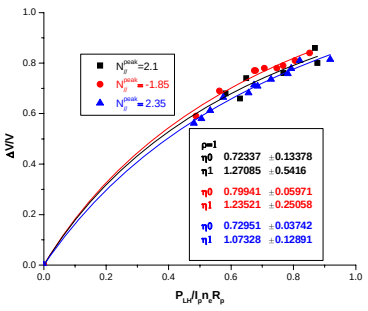

FIG. 15 CD efficiency vs $N_{//}^{peak}$

hence affecting drive efficiency, in agreement with code simulations. The current drive efficiency is affected by density. The effect of power spectrum on current drive efficiency is small, possibly due to low plasma temperature.

In the present parameters in EAST, the current drive efficiency is relative low. This is mainly due to low plasma temperature, since the experimentally obtained current drive efficiency in JT-60U and JET much depends on plasma temperature [23]. This could be improved with the improvement of plasma parameter in future.

Acknowledgements: This work is supported by the National Natural Science Foundation of China under Grant No. 10875149 and 10928509, the ITER Relevant Foundation in China (Grant No 2010GB105000), and the Dean Foundation of Hefei Institute of Physical Science, Chinese Academy of Science. In addition, one of the authors, B J Ding, would like to thank the members of EAST Team for their cooperation and kindly help.

References:

[1] Jobes F.C. *et al* 1985 *Phys. Rev. Lett.* **55** 1295
[2] Leuterer F. *et al* 1985 *Phys. Rev. Lett.* **55** 75
[3] Takase Y. *et al* 1987 *Phys. Fluids* **30** 1169
[4] Leuterer F. *et al* 1991 *Nucl. Fusion* **31** 2315
[5] Hoang G T, Gil C, Joffrin E, *et al* 1994 *Nucl. Fusion* **34** 75.
[6] Ide S, Fujita T, Naito O *et al* 1996 *Plasma Phys. Control. Fusion* **38** 1645.
[7] Pamela J and JET EFDA Contributors 2003 *Nucl. Fusion* **43** 1540.
[8] Romanelli F. FTU Team and ECRH Team 2002 *Overview of the FTU results* Fusion Energy 2002 (*Proc. 19th Int. Conf. Lyon, 2002)* (Vienna: IAEA) CD-ROM file OV/4-5 and http://www.iaea.org/programmes/ripc/physics/fec2002/html/fec2002.htm
[9] Wan Y.X. *et al* 2000 *Nucl. Fusion* **40** 1057

[10] Weng P.D. *et al* 2005 *Fusion Eng. Des.* **75–79** 143

[11] Fu P. *et al* 2006 *Nucl. Fusion* **46** S85
[12] Liu X.N. *et al* 2006 *Nucl. Fusion* **46** S90
[13] Wan Y.X. *et al* 2006 *Plasma Sci. Technol.* **8** 253
[14] Brambilla M. 1976 *Nucl. Fusion* 16 47
[15] Petržilka V. A., Leuterer F., Söldner F.-X., *et al* 1991 *Nucl. Fusion* **31** 1758.
[16] Bell R.E., Bernabei S., Greenough N.,*et al* 1994 *Nucl. Fusion* **34** 271.
[17] Fisch N J, 1985 *Phys. Fluids* **28** 245.
[18] Gituzzi G, Barbato E, Bernabei S, Cardinali A, 1997, *Nucl. Fusion* **37** 673.
[19] Spitzer L, Harm R, 1953 *Phys. Rev* **89** 977.
[20] STIX T. H. The Theory of Plasma Waves, McGraw-Hill, New York(1962).
[21] Karney C F, Fisch N J, 1986 *Phys. Fluids* **29** 180.
[22] Karney C F, Fisch N J and Jobes F C, 1985 *Phys. Rev. A* **32** 2554.
[23] SHI B.R. 1999 *Magnetic Confinement Fusion Principles and Practice* Atomic Energy Press, Beijing (in Chinese).